To cite this article: WANG X Q, LAI S G, XIAO Z J. The influence of bailers on the hydrodynamic performance of the seaplane[J/OL]. Chinese Journal of Ship Research, 2021, 16(2). http://www.ship-research.com/EN/Y2021/V16/I2/30.

DOI: 10.19693/j.issn.1673-3185. 01798

The influence of bailers on the hydrodynamic performance of the seaplane

WANG Xiaoqiang[1], *LAI Shuguang*[*2], *XIAO Zhijian*[3, 4]

1 Wuhan Second Military Representative Office, Naval Armament Department of PLAN, Wuhan 430064, China

2 China Ship Development and Design Center, Wuhan 430064, China

3 China Special Vehicle Research Institute, Jingmen 448035, China

4 Aviation Key Scientific and Technological Laboratory of High Speed Hydrodynamic, Jingmen 448035, China

Abstract: [**Objectives**] The hydrodynamic performance under different bailer conditions based on numerical and experimental methods was investigated. [**Methods**] The hydrodynamic performance of the seaplane with different displacements at different speeds was studied using an experimental method, and the viscous flow field of the seaplane under three conditions (without bailer, bailer closed, and bailer lowered) at different speeds was computed based on CFD methods. [**Results**] The results show that at the same displacement, the total resistance and heave amplitude of the seaplane increase, but the trim angle decreases as the speed increases; when displacement increases, the total resistance, trim angle and heave amplitude of the seaplane all increase; when the bailer lowers, the total resistance and heave amplitude of the seaplane increase, yet the trim angle decreases; the effect of the bailer on the hydrodynamic performance is not obvious when it is closed. [**Conclusions**] The results of this paper are of great significance to the optimal design of the seaplane bailer.

Key words: seaplane; bailer; water-drawing efficiency; water-drawing load; hydrodynamic performance

CLC number: U661. 3

0 Introduction

Compared with traditional means of firefighting, large seaplanes for forest firefighting have multiple advantages, such as high mobility, high speed, and large water carrying capacity [1]. By far, domestic and foreign scholars have completed the development of a series of seaplane fire-extinguishing systems that rely on drawing and dropping water after years of research and practice, and achieved significant results in the practical application. In terms of water-drawing devices for seaplanes, very few relevant studies and literature have been published in China and abroad, and they mainly focused on the overall aerodynamic and hydrodynamic performance of seaplanes. In 1959, Mottard[2] investigated the effect of waves on resistance during seaplane takeoff. In 2012, Wang et al. [3] obtained a mathematical model of the water-dropping algorithm based on the continuously computed release point (CCRP) principle of the bomb. In the end, a water-dropping algorithm for large fire-fighting aircrafts was proposed in light of the theory of free turbulent jet. In 2015, Huang et al. [4-5] conducted an in-depth study on the wave test technique of amphibious aircraft models, the motion response of the aircraft on waves, and the hydrodynamic moment characteristics of the hull. In 2019, Duan et al. [6] investigated the aerodynamic and hydrodynamic performance of seaplanes when moored in water based on CFD methods.

Due to the lack of relevant studies, the following research is proposed based on the design needs of the seaplane bailer: Variation of resistance and atti-

Received: 2019 − 10 − 17 **Accepted:** 2020 − 05 − 12

Authors: WANG Xiaoqiang, male, born in 1981, Ph.D., engineer
LAI Shuguang, male, born in 1991, master, engineer
XIAO Zhijian, male, born in 1992, master, engineer

***Corresponding author:** LAI Shuguang

tude with the velocity of the aircraft at different displacements under the lowered bailer condition is studied through conducting towing test on calm water. Variation of water-drawing efficiency, water-drawing load, and additional pitching moment of bailer with speed is investigated through numerical simulation analysis. The hydrodynamic characteristics of the seaplane, such as resistance, heave, and trim under three conditions (without bailer, bailer closed, and bailer lowered) are also discussed.

1 Geometric models and methods

1.1 Geometric models

The towing test on calm water (EFD) and simulation calculation (CFD) were carried out with a seaplane unpowered model as the experiment and simulation object. The working conditions of test and numerical calculation are shown in Table 1. First, towing test on calm water was conducted with the seaplane at three displacements ($0.79\varDelta_a$, $0.85\varDelta_a$, and $\varDelta_a$) with the lowered bailer. Subsequently, simulations of the hydrodynamic performance of the seaplane with a displacement of $\varDelta_a$ were carried out for three conditions: without bailer, bailer closed, and bailer lowered. The experiment model and simulation object are shown in Fig. 1. The geometrical diagrams of the three operating conditions are shown in Fig. 2.

1.2 Mesh division

In this paper, cut volume meshes are used to generate high-quality wall meshes. Complex surfaces or areas with severe flow separation, such as the free surface, the draught area of the fuselage step, and control surfaces, are densified by means of volume control. Overlapping meshes are adopted to solve aircraft motion problems. At the same time, the near-wall surfaces within the overlapping regions are densified to accurately capture the near-wall flow. In order to ensure the accuracy of the aerodynamic and hydrodynamic performance calculation results, the settings of the control surfaces and hull boundary layers are considered respectively. The average wall $y+$ value of each control surface is 1, and the number of boundary layers is 15. The average wall $y+$ value of the fuselage surface is 5, and the number of boundary layers is 8. The surface meshes of the model are shown in Fig. 3.

Table 1 Conditions of experiment and numerical simulation

Working condition	Displacement	Bailer status	Speed/ ($m\cdot s^{-1}$)	Research method
1	$0.79\varDelta_a$	Lowered	8	EFD
2	$0.85\varDelta_a$	Lowered	9	EFD
3	$\varDelta_a$	Lowered	10	EFD
4	$\varDelta_a$	No bailer	11	CFD
5	$\varDelta_a$	Closed	12	CFD
6	$\varDelta_a$	Lowered	13	CFD

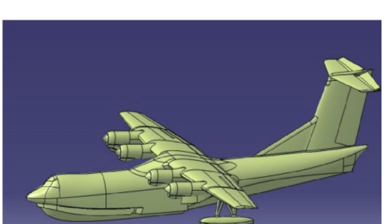

Fig. 1 Features of the studied model

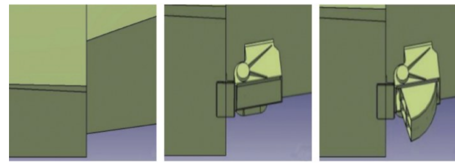

(a) No bailer (b) Bailer closed (c) Bailer lowered

Fig. 2 Features of bailer under three conditions

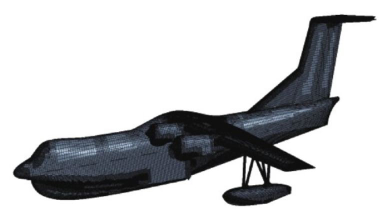

Fig. 3 Mesh distributions of the model

The mesh computational domain is $-1.0L \leqslant x \leqslant 4.5L$, $-1.5L \leqslant y \leqslant 1.5L$, $-1.0L \leqslant z \leqslant 1.0L$, where x, y, and z are the coordinate values of the length, width, and height of the computational domain, and L is the total length of the seaplane. Due to the geometric symmetry of the model, half of the model can be used for simulation. Therefore, the boundary conditions for the plane of symmetry are used. The upstream inlet uses velocity inlet, whereas the downstream outlet uses pressure outlet. The upper boundary, side, and lower boundary adopt velocity-inlet boundary conditions. Wall boundary conditions without slippage can be defined on the surface of the model. The applied boundary conditions of the computational domain are set as shown in Fig. 4.

The RANS method is used to solve the problem, and the turbulence model adopts the SST k-ω turbulence model [7]. The second-order upwind finite volume method (FVM) is used to discretize the control equations. The convection term is discretized in a

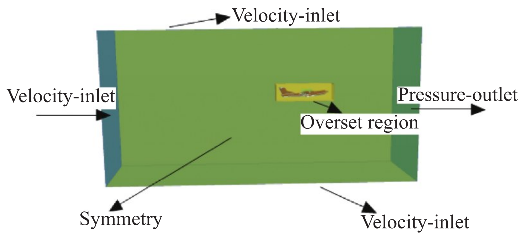

Fig. 4 The applied boundary conditions

Fig. 5 Experimental layout

second-order upwind scheme, and the diffusion term is discretized in a second-order scheme. Free surface capture adopts the volume of fluid (VOF) technology for two-phase flows.

2 Towing test

2.1 Test design

Real seaplanes store the drawn water in the specific water tank. In this test, however, the water flowing into the bailer is discharged from the side of the aircraft through the piping of the water-drawing system. As needed, a specific mass of water needs to be pre-filled into the model tank before the trailer starts.

The test is conducted on the protrusive part of the trailer, as shown in Fig. 5. The propeller of the model shown in Fig. 5 is fixed and therefore would not affect the comparison and analysis of simulation and test results. Protrusive experimental devices mainly include a trailer, a protrusive device, a motion device, and a limit device. The protrusive device is cemented to the trailer to extend the position of the test model forward to the front of the trailer. The motion device is an installation device that guarantees the mobility of the aircraft, including a trolley, a heave rod, and a center of gravity connecting rod. The trolley can move forwards and backwards within a certain range along the heading on the protrusive edge to ensure that the model can move freely along the heading. The heave rod passes through the trolley and is consolidated to the upper end of the center of gravity connecting rod. During the test, the heave rod translates vertically with the model to ensure that the model can heave freely. The lower end of the center of gravity connecting rod is hinged with the model at the center of gravity position to guarantee its pitching motion. Moreover, the limit device is mainly to limit the yaw movement of the model to avoid the danger of the model colliding with the pool wall during the model test. The limit function is realized via the navigation lever.

2.2 Test data

The resistance and attitude test results for working conditions 1 to 3 are shown in Fig. 6 to Fig. 8. As can be seen from the figures, the dimensionless total drag coefficient (F_t/Δ) and dimensionless heave coefficient (*Heave*/*L*) increase, whereas the trim angle decreases for each working condition as the velocity V goes up. The total dimensionless drag coefficient, trim angle, and dimensionless heave coefficient also rise as the displacement increases. In this paper, rising and trim by stern are positive.

3 Numerical method simulation

3.1 Numerical method verification

With condition 3 and condition 6 as examples, the verification of numerical calculation methods is carried out by comparing the experimental and simulation results of the seaplane model with the low-

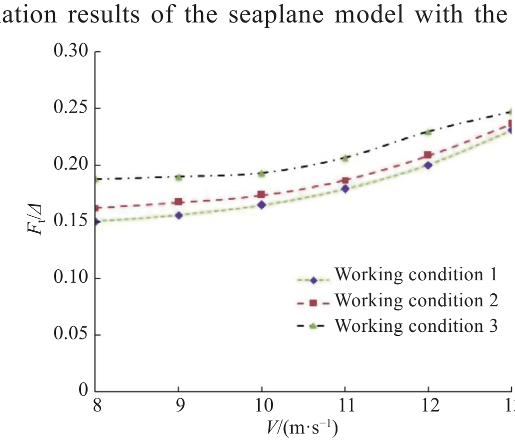

Fig. 6 Experimental dimensionless total drag coefficient

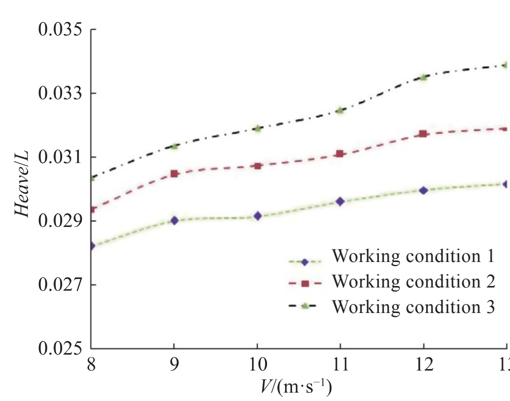

Fig. 7 Experimental dimensionless heave coefficient

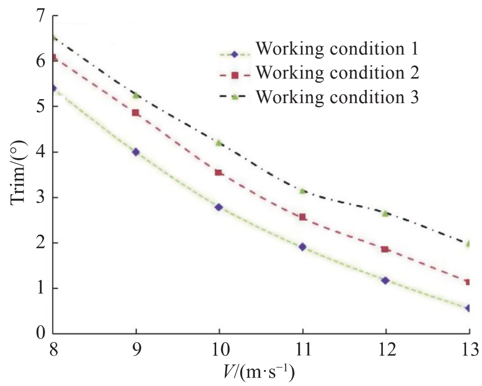

Fig. 8 Experimental trim angle

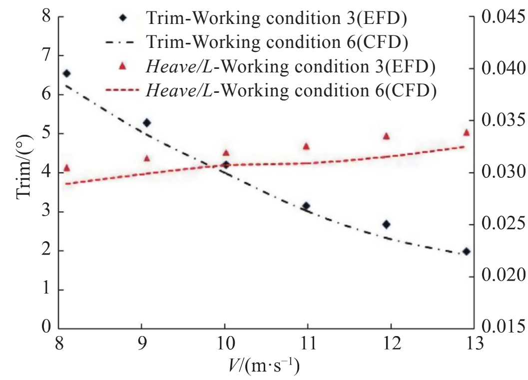

Fig. 10 Comparison of experimental and computed attitudes

ered bailer. The geometric model and meshing are described in Section 2.

As is shown in Fig. 9 and Fig. 10, in the test, the trends of the dimensionless total drag coefficient, dimensionless heave coefficient, and trim angle at different speeds in the test correspond with the numerical calculations, verifying the rationality and accuracy of the calculation method proposed here. As can be seen in Fig. 9, the calculated water resistance is less than the test value, which may be because the effect of the pool wall is not considered in the numerical calculations compared with physical experiments. At the same time, the free surface capture model of the software cannot fully simulate the spattering resistance of the model gliding at high speed.

3.2 Water-drawing efficiency and water-drawing load of the bailer

Since the specified amount of displacement needs to be completed within a specified time, this paper analyzes the variation of the water-drawing efficiency of the bailer with speed by computing the flow rate of the bailer. As can be seen from Fig. 11, the flow rate Q (unit: kg/s) of the bailer increases with the velocity V (unit: m/s), and the two have a non-linear relationship. Therefore, a quadratic polynomial function is used for fitting, and we get

$$Q = -0.015V^2 + 0.596V - 1.841 \tag{1}$$

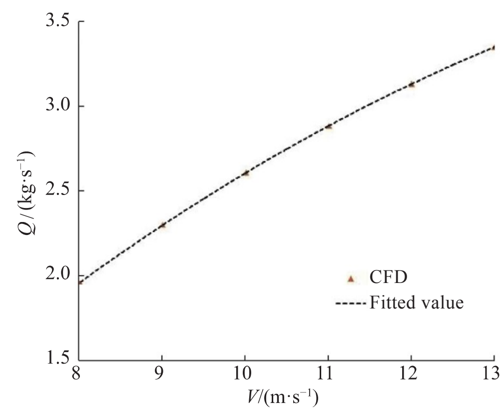

Fig. 11 Comparison of computed mass flow and fitted value

A comparison between the computed and fitted values of the flow rate shows that the relationship between the flow rate and the velocity of the bailer can be well fitted into a quadratic function. The volume fraction distribution of the bailer inlet at different speeds is shown in Fig. 12. The wetted surface area of the bailer varies with the speed, so the water-drawing efficiency is not proportional to the speed.

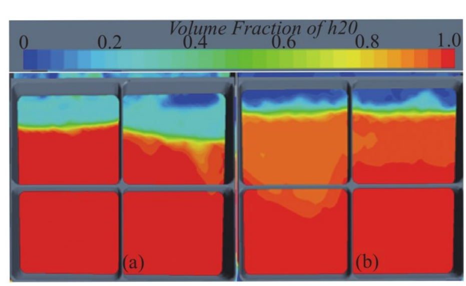

Fig. 12 Volume fraction of water at speed of 8 m/s (a) and 13 m/s (b)

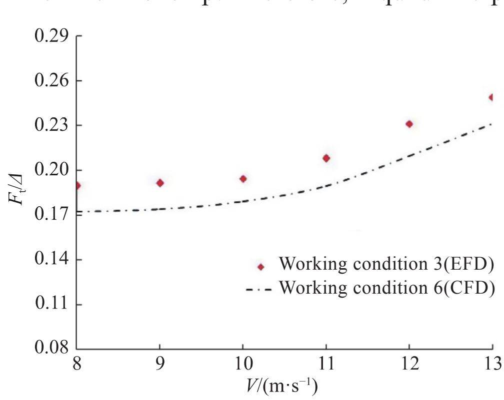

Fig. 9 Comparison of experimental and computed dimensionless total drag coefficient

Apart from guaranteeing the water-drawing efficiency during the water-drawing process, it is also necessary to take into consideration the water-drawing load and the additional pitching moment generated to avoid structural damage and loss of control of the aircraft. With V = 13 m/s as an example, it can be seen from Fig. 13 that with the lowered bailer, the pressure inside the bailer is obviously larger than that outside the bailer. The load of the bailer can be resolved into horizontal resistance (F_x) and vertical downward pulling force (F_z). Fig. 14 indicates that the lift resistance coefficient is within 0.002 when the bailer closes, and the load on the bailer is almost negligible. With the lowered bailer, the drag coefficient increases from 0.02 to 0.051, and the lift coefficient increases from 0.018 to 0.044, so the load on the bailer goes up significantly. With the increase in speed, F_x and F_z both demonstrate nonlinear growth. Fig. 15 shows that the additional pitching moment coefficient generated by the bailer when it closes is within 0.20, which is almost negligible. In contrast, the additional pitching moment coefficient increases non-linearly from 1.59 to 3.97 with the speed generated by the bailer on the fuselage when it lowers. Therefore, the bailer design should focus on both the load and additional pitching moment of the bailer when it lowers.

3.3 Effect of the bailer on the total resistance of the aircraft

The computed variation curves of the dimensionless total drag coefficient with velocity for the three states are shown in Fig. 16. As can be seen from

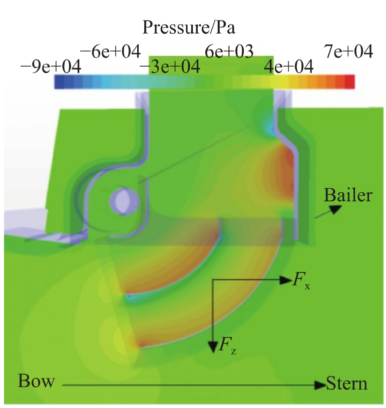

Fig. 13 Internal and external pressure distribution of bailer at the speed of V = 13 m/s

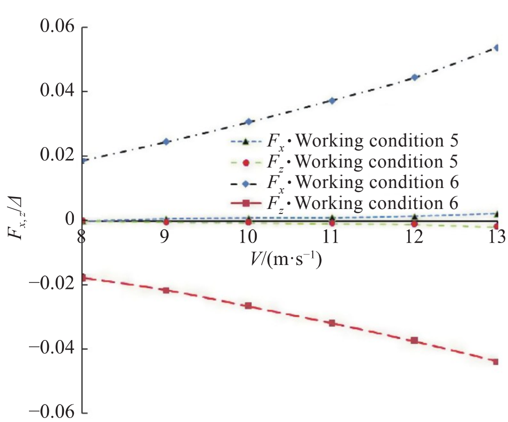

Fig. 14 Computed dimensionless force coefficients

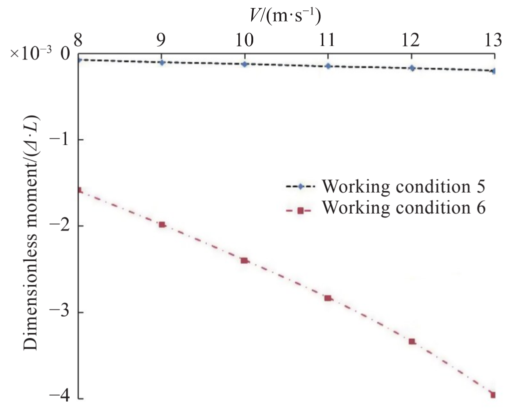

Fig. 15 Computed dimensionless moment coefficients

Fig. 16, the total resistance in the case of no bailer is relatively close to that of the closed bailer. When the speed increases, both curves show a trend of first decreasing and then increasing with a very small variation. In contrast, the total resistance increases significantly when the bailer lowers and grows approximately quadratically with speed. Fig. 17 gives the variation of the growth rate of resistance with the velocity caused by the bailer being closed or lowered compared with that in the case without the bailer. With higher speed, the resistance increases less when the bailer closes, which is from 2.6% to 6.0%. In contrast, it increases significantly, from 47.2% to 95.7%, when the bailer lowers. Therefore, when the bailer closes, the influence on the total resistance is minimal compared with that in the case with no bailer. In contrast, the resistance goes up sharply as the bailer is closed, and the growing rate increases with respect to the speed.

3.4 Influence of bailer on skidding stability

Fig. 18 shows the variation curve of the trim angle of the fuselage with velocity in the three cases. From Fig. 18, it can be seen that the trim angle of the fuselage reduces with the increasing velocity un-

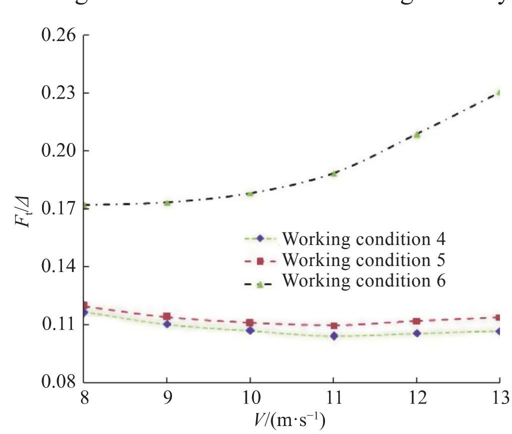

Fig. 16 Variation of dimensionless total drag coefficient with respect to speed

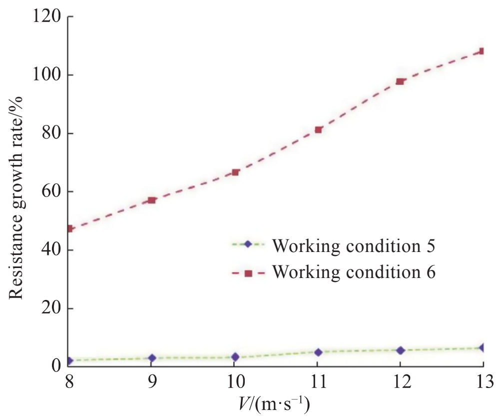

Fig. 17 Variation of dimensionless total drag coefficient with respect to speed

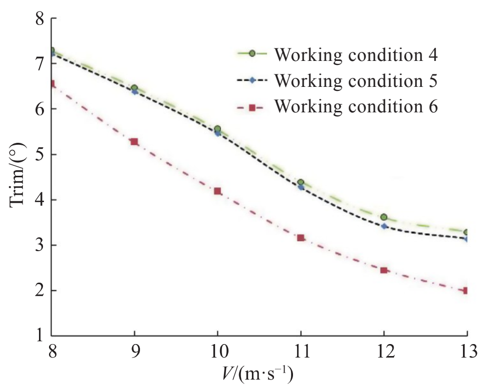

Fig. 18 Variation of trim angle with respect to speed under different conditions

der all three conditions. The trim angle of the fuselage shows a very small change when the bailer is closed but narrows significantly when the bailer is lowered compared with that in the case with no bailer. As is seen in Fig. 15, when the bailer lowers, it produces a large additional pitching moment, which suppresses the stern trim of the fuselage. Hence, the amplitude of the trim angle significantly decreases when the bailer lowers. The additional pitching moment with the closed bailer is very small, so the difference between the trim angle amplitudes for a closed bailer and no bailer is minimal.

The variation curves of the dimensionless heave coefficient of the fuselage with the increasing speed for the three statuses are shown in Fig. 19. It can be seen that the heave amplitudes of the fuselage in these three cases decrease with the increase in speed. The gap between the trim angles with the bailer closed and without the bailer is small, while the trim angle when the bailer lowers is greatly larger than in the other two cases. Fig. 14 shows that the bailer is pulled downwards when it lowers. However, analysis of the load of the entire water-drawing system (bailer and pipeline) shows that a lift of 2.3% to 5.1% within the computed speed range is generated. Therefore, the fuselage rises much higher than in the other two cases when the bailer lowers. In contrast, with the closed bailer, the water flow does not pass through the water-drawing system, and the bailer is behind the fuselage step with minimal vertical force. Therefore, the heave amplitude of the fuselage when the bailer closes is similar to that with no bailer.

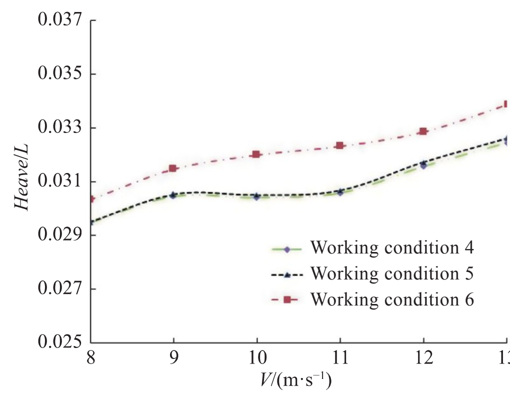

Fig. 19 Variation of *Heave*/*L* with respect to speed at different conditions

Fig. 20 and Fig. 21 show the simulation and test results of the free surface distribution at the speed of $V = 13$ m/s when the bailer lowers. In Fig.20, H and $L2$ are the height of free-surface and the length of the bucket respectively. According to the simulation results shown in Fig. 20, the Kelvin angle generated by the seaplane when gliding at high speed is small, and the emerging waves are mainly concentrated in the rear fuselage. It can be observed that the water wave sprayed from the step area is close to the surface of the rear body, leading to an adsorption phenomenon. The amplitude of the emerging waves increases from the hull step to the tail and then decreases, and the water is ejected from the spout of the water-drawing system and then falls into the water surface. Similar phenomena as described above can also be observed from the test results shown in Fig. 21. In a nutshell, the distribution of the free surface from the test is in accordance with the simulation.

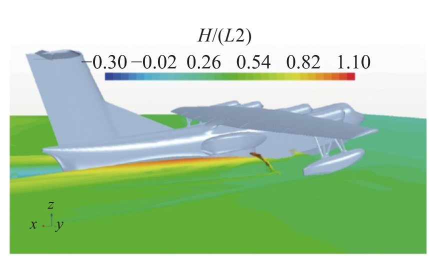

Fig. 20 Computed free surface at the speed of $V = 13$ m/s

Fig. 21 Experimental free surface at the speed of $V = 13$ m/s

4 Conclusion

In this paper, the main conclusions from experiments and numerical computations are as follows.

1) The test results show that at the same displacement, the total resistance and heave amplitude increase, but the trim angle decreases as the speed goes up. The total resistance, heave amplitude, and trim angle all increase when the displacement increases.

2) The flow rate of the bailer increases with the speed, and their relationship is non-linear. A quadratic function can be used to well fit the relationship between the flow rate of the bailer and velocity. When the bailer lowers, its drag coefficient increases from 0.02 to 0.051, the lift coefficient increases from 0.18 to 0.44, and the additional pitching moment coefficient increases from 1.59 to 3.97. All of the three grow non-linearly with the increasing speed. The forces and moments are negligible when the bailer closes.

3) Simulation results show that the total resistance of the seaplane increases significantly as the bailer lowers. As the speed increases, the total resistance increment increases from 47.2% to 95.7% with respect to the case without a bailer. Meanwhile, the heave amplitude of the seaplane also increases, but the trim angle decreases. In contrast, the influence of the bailer on the hydrodynamic performance of the seaplane can be ignored when the bailer closes.

References

[1] CHU L T. Seaplane hydrodynamic design [M]. Beijing: Aviation Industry Press, 2014: 169−171 (in Chinese).

[2] MOTTARD E J. A brief investigation of the effect of waves on the take-off resistance of a seaplane: NASA TN-D-165 [R]. Washington, DC: NASA, 1959.

[3] WANG Y L, CAI Z Y, ZHAO H J. Study of the algorithm for dropping water with air tanker [J]. Microcomputer Information, 2012, 28(9): 265−266, 276 (in Chinese).

[4] HUANG M, WU B, JIANG R, et al. Experimental study on motion response of a seaplane on waves [J]. Journal of Experiments in Fluid Mechanics, 2015, 29 (3): 41−46 (in Chinese).

[5] HUANG M, LIAN Z D, ZUO Z B, et al. Study of scaled model tank tests in waves of an amphibian [J]. Aeronautical Science & Technology, 2016, 27(1): 74−78 (in Chinese).

[6] DUAN X P, SUN W P, WEI M, et al. Numerical simulation of amphibious aircraft taxiing at high speed on water using OpenFoam [J]. Acta Aeronautica et Astronautica Sinica, 2019, 40(1): 522330 (in Chinese).

[7] ZHANG L, CHENG Y S, WANG F X. Coupled hydrodynamic and aerodynamic performance analysis of seaplane take-off process in calm water [J]. Science Technology and Engineering, 2018, 18(11): 190−195 (in Chinese).

汲水斗对水面飞行器水动力性能的影响

王晓强[1]，来曙光[*2]，肖志坚[3,4]

1 海军装备部驻武汉地区第二军事代表室，湖北 武汉 430064

2 中国舰船研究设计中心，湖北 武汉 430064

3 中国特种飞行器研究所，湖北 荆门 448035

4 高速水动力航空科技重点实验室，湖北 荆门 448035

摘 要：[**目的**]基于数值和试验方法研究汲水斗不同状态下水面飞行器的水动力性能变化规律。[**方法**]首先，通过试验方法研究水面飞行器放下汲水斗时在不同速度及不同排水量下的水动力性能；然后，采用CFD数值方法求解不同速度下，无、收起和放下汲水斗3种情况下水面飞行器的黏性绕流场。[**结果**]结果显示，随着速度的增大，在相同汲水量下，水面飞行器的总阻力、升沉幅度均随之增大，纵倾角减小；随着汲水量的增大，其总阻力、纵倾角和升沉幅度增大；汲水斗放下时水面飞行器的总阻力明显增大，升沉增大，但纵倾角减小；汲水斗收起时对水面飞行器的水动力性能影响不大。[**结论**]所得研究结果对水面飞行器汲水斗的优化设计具有重要指导意义。

关键词：水面飞行器；汲水斗；汲水效率；汲水载荷；水动力性能